

Realization of a 9-axis Inertial Measurement Unit toward Robotic Applications

Jau-Ching Lu

Department of Mechanical Engineering,
 National Taiwan University
 Taipei, Taiwan
 Corresponding email:
peichunlin@ntu.edu.tw

Chia-Hung Tsai

Department of Mechanical Engineering,
 National Taiwan University
 Taipei, Taiwan
 Corresponding email:
peichunlin@ntu.edu.tw

Pei-Chun Lin*

Department of Mechanical Engineering,
 National Taiwan University
 Taipei, Taiwan
 Corresponding email:
peichunlin@ntu.edu.tw

Abstract—We report on the integration of a 9-axis IMU with a 2-axis inclinometer which yields precise body orientation with respect to the gravity. Thus, a pre-treatment of gravity compensation for accelerometers of the previously-developed 9-axis IMU can be done correctly in real-time. The integrated system is capable of delivering desired linear acceleration, angular acceleration, and angular velocity states in normal gravitational environment. In addition, the system also releases the requirement of accelerometer installation at the center of mass as in the traditional IMU, and it derives the angular acceleration via simple matrix operation. Thus, the proposed system can potentially be utilized in the legged robots where the COM moves due to motion of the limbs.

Keywords—inertial measurement unit; accelerometer; gyroscope; body state

I. INTRODUCTION

For several decades, inertial sensors [1-3] have been one of the important categories of sensors utilized in various applications, including navigation (robots, vehicles, rockets, and etc) [2-4], state estimation for motion analysis [5] or dynamic modeling, microsurgery [6], and sports injury avoiding [7-8]. In modeling dynamics of legged robots[9-10], information of external forces, position and orientation states (including their 1st/2nd derivatives) are usually required as essential information for constructing low degree-of-freedom (DOF) 2nd-order dynamic models, and the inertial measurement unit (IMU) is an appropriate choice to provide some essential states.

Recently, we have developed a 9-axis IMU containing 3-axis angular velocity measurements from the rate gyros and 6-axis linear acceleration measurements from accelerometers at three distinct locations [11]. This system provides instant angular acceleration derivation via linear operation without any differentiation or integration as in the traditional IMU, which is comprised of a 3-axis accelerometer installed at center of mass (COM) and a 3-axis rate gyro. In addition, the flexible positioning of three 2-axis accelerometers in the 9-axis IMU also releases the strong constraint of accelerometer installation at COM as the traditional IMU does. Here, we

investigate the integration of this 9-axis IMU with a 2-axis inclinometer which yields precise body orientation with respect to the gravity. Thus, a pre-treatment of gravity compensation for the accelerometers can be done correctly in real-time. The proposed method significantly improves the performance than that derived from gyro signals, because the later one induces unbounded orientation error due to integration of angular velocity.

Section II briefly introduces the previously-developed 9-axis sensory system, followed by the mechanism of gravity compensation which utilizes the 2-axis inclinometer. Section III reports the results of experimental evaluation, and Section IV concludes the work.

II. CONSTRUCTION OF THE SENSING SYSTEM

A brief review of system construction is listed below. In Newton dynamics, the acceleration vector, \mathbf{a}_p , in an inertial frame \mathcal{W} of a point, p , attached to an accelerating body frame \mathcal{B} with origin, o , as shown in Fig. 1, is a function of the body's angular velocity, $\boldsymbol{\omega}$, angular acceleration, $\dot{\boldsymbol{\omega}}$,

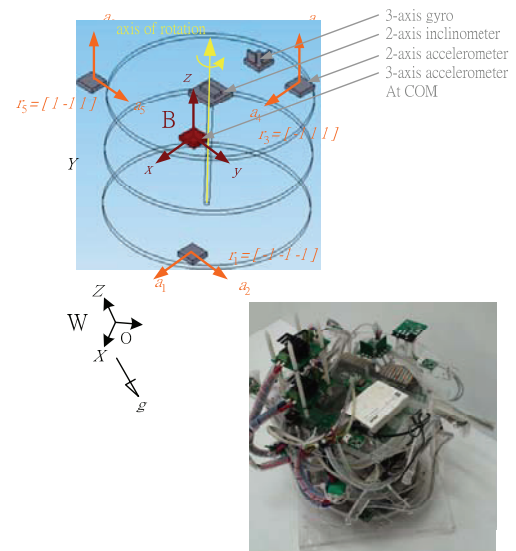


Figure 1. Top: sketch of the 9-axis IMU with a 2-axis inclinometer and bottom: the experimental apparatus.

This work is supported by National Science Council (NSC), Taiwan, under contract NSC 98-2218-W-002-034.

and linear acceleration of the body origin, \mathbf{a}_o , given by

$$\mathbf{a}_p = \mathbf{a}_o + \dot{\boldsymbol{\omega}} \times \mathbf{r}_{op} + \boldsymbol{\omega} \times (\boldsymbol{\omega} \times \mathbf{r}_{op}) + (\ddot{\mathbf{r}}_{op})_r + 2\boldsymbol{\omega} \times (\dot{\mathbf{r}}_{op})_r, \quad (1)$$

where \mathbf{r}_{op} , the position vector of point p relative to o , is presumed known *a priori*. In general, we are interested in utilizing the measurements from commercially available low-cost accelerometers and gyros to derive 9 unknown scalar body states on the right side of the equation, including the COM linear acceleration, \mathbf{a}_{COM} ,

$$\mathbf{a}_0 = \mathbf{a}_{COM} = [a_x \quad a_y \quad a_z]^T \quad (2a)$$

and the angular acceleration $\dot{\boldsymbol{\omega}}$ and angular velocity $\boldsymbol{\omega}$ of the moving body.

$$\boldsymbol{\omega} = [\omega_x \quad \omega_y \quad \omega_z]^T \quad (2b)$$

$$\dot{\boldsymbol{\omega}} = [\dot{\omega}_x \quad \dot{\omega}_y \quad \dot{\omega}_z]^T. \quad (2c)$$

In a strapdown system the sensors are mounted rigidly on the body, so \mathbf{r}_{op} is a fixed vector viewed from \mathcal{B} frame, and the last two terms in (1) are zeros. In general, three mutually orthogonal 1-axis angular velocity measurements from the rate gyros can readily provide $\boldsymbol{\omega}$,

$$\boldsymbol{\omega}_m = [\omega_1 \quad \omega_2 \quad \omega_3]^T. \quad (3)$$

Thus, with additional six 1-axis gravity-compensated acceleration measurements $a_{j,j=1-6}$,

$$\mathbf{a}_m = [a_1 \quad a_2 \quad a_3 \quad a_4 \quad a_5 \quad a_6]^T, \quad (4)$$

we are able to construct six scalar equations based on (1) shown as follows,

$$\mathbf{a}_m = S(r)x_{var} + W(r) \begin{bmatrix} \omega_1^2 + \omega_2^2 \\ \omega_1^2 + \omega_3^2 \\ \omega_2^2 + \omega_3^2 \\ \omega_1\omega_2 \\ \omega_1\omega_3 \\ \omega_2\omega_3 \end{bmatrix}. \quad (5)$$

The ‘‘structure matrix’’ $S(r)$ is

$$S(r) = \begin{bmatrix} 1 & 0 & 0 & 0 & r_{1z} & -r_{1y} \\ 0 & 1 & 0 & -r_{2z} & 0 & r_{2x} \\ 0 & 0 & 1 & r_{3y} & -r_{3x} & 0 \\ 1 & 0 & 0 & 0 & r_{4z} & -r_{4y} \\ 0 & 1 & 0 & -r_{5z} & 0 & r_{5x} \\ 0 & 0 & 1 & r_{6y} & -r_{6x} & 0 \end{bmatrix}, \quad (6a)$$

and

$$W(r) = \begin{bmatrix} 0 & 0 & -r_{1x} & r_{1y} & r_{1z} & 0 \\ 0 & -r_{2y} & 0 & r_{2x} & 0 & r_{2z} \\ -r_{3z} & 0 & 0 & 0 & r_{3x} & r_{3y} \\ 0 & 0 & -r_{4x} & r_{4y} & r_{4z} & 0 \\ 0 & -r_{5y} & 0 & r_{5x} & 0 & r_{5z} \\ -r_{6z} & 0 & 0 & 0 & r_{6x} & r_{6y} \end{bmatrix}, \quad (6b)$$

where r_{jk} denotes a scalar component of the position vector of sensor j with direction k [11]. Thus, the remaining 6 scalar unknowns of linear and angular acceleration states, \mathbf{a}_o (a_x, a_y, a_z) and $\dot{\boldsymbol{\omega}}$ ($\dot{\omega}_x, \dot{\omega}_y, \dot{\omega}_z$) defined in x_{var} ,

$$x_{var} = [a_x \quad a_y \quad a_z \quad \dot{\omega}_x \quad \dot{\omega}_y \quad \dot{\omega}_z]^T, \quad (7)$$

can be derived by the matrix operation,

$$x_{var} = S(r)^{-1}(\mathbf{a}_m - W(r)\boldsymbol{\omega}_m). \quad (8)$$

Equation (8) reveals that the desired linear and angular acceleration states are determined by both accelerometer and rate gyro readings as well as the positions of accelerometers. Previously[11], we found that the best configuration of the sensors (i.e. with best condition number of $S(r)$, which yields the best quality of matrix inversion.) shows certain symmetry of sensor positions with respect to the origin as depicted in Fig. 1. In this configuration, the sensing directions of accelerometers $\{a_1, a_4\}$, $\{a_2, a_5\}$, $\{a_3, a_6\}$ are toward x, y, z principal axes of the body frame, respectively. Assuming the structure matrix $S(r)$ with best configuration is denoted as $S(r_{best})$ and assuming that of $W(r)$ is denoted as $W(r_{best})$, following (8) the quantitative relation between the acceleration outputs and the sensor inputs of three 2-axis IMU is:

$$x_{var} = S(r_{best})^{-1}(\mathbf{a}_m - W(r_{best})\boldsymbol{\omega}_m)$$

$$\begin{bmatrix} a_x \\ a_y \\ a_z \\ \dot{\omega}_x \\ \dot{\omega}_y \\ \dot{\omega}_z \end{bmatrix} = \begin{bmatrix} m & 0 & 0 & m & 0 & 0 \\ 0 & m & 0 & 0 & m & 0 \\ 0 & 0 & m & 0 & 0 & m \\ n & n & n & -n & -n & -n \\ -n & -n & n & n & n & -n \\ n & -n & n & -n & n & -n \end{bmatrix} \begin{bmatrix} a_1 \\ a_2 \\ a_3 \\ a_4 \\ a_5 \\ a_6 \end{bmatrix}, \quad (9)$$

$$= \begin{bmatrix} 0 & 0 & 1 & 0 & 0 & 0 \\ 0 & 1 & 0 & 0 & 0 & 0 \\ -1 & 0 & 0 & 0 & 0 & 0 \\ 0 & 0 & 0 & -1 & -1 & 0 \\ 0 & 0 & 0 & 1 & 0 & 1 \\ 0 & 0 & 0 & 0 & -1 & 1 \end{bmatrix} \begin{bmatrix} \omega_1^2 + \omega_2^2 \\ \omega_1^2 + \omega_3^2 \\ \omega_2^2 + \omega_3^2 \\ \omega_1\omega_2 \\ \omega_1\omega_3 \\ \omega_2\omega_3 \end{bmatrix}, \quad (9)$$

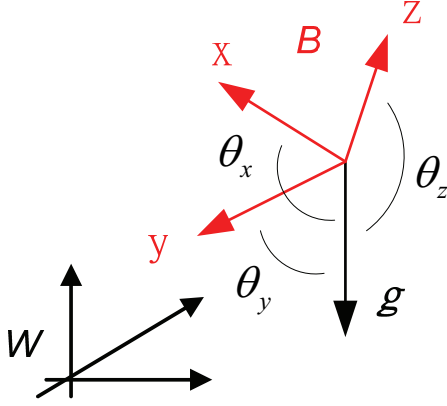


Figure. 2. The angles defined by the property of direction cosine.

where $m=0.5$ and $n=0.25$. Since the optimal configuration is symmetric with respect to three principal axes, similar composition of three components of state is expected and (9) confirms this expectation. The difference in sign is resulted from the relative position of these three sensory suites to the three principal axes and the assignment of sensing directions, which are all toward positive directions of principal axes as shown in Fig. 1.

Equation (9) shows that besides gyro's effect, the linear acceleration $a_{i,i=x,y,z}$ is only affected by the accelerometers measuring in the same direction, and these two readings affect the measurements of a_i equally with scaling factor $m=0.5$. On the other hand, equation (9) shows that the angular acceleration $\dot{\omega}_{i,i=x,y,z}$ is affected by all accelerometer measurements, and effect of individual accelerometer to $\dot{\omega}_i$ is down to a quarter $n=0.25$. Interestingly, the deviation of the angular acceleration from accelerometer measurements shown in (9) is in some sense like a differential process, which means two accelerometer measurements in the same sensing direction will be multiplied by constants with different sign before addition. For example, in derivation of $\dot{\omega}_x$, the first three $a_{j,j=1,2,3}$ multiple by n but the other three $a_{j,j=4,5,6}$ multiple by $-n$,

$$\dot{\omega}_x = n(a_1 - a_4) + n(a_2 - a_5) + n(a_3 - a_6). \quad (10)$$

This fact is true for $\dot{\omega}_i$ in all three directions. Because the accelerometers with the same sensing direction measure the same gravity-induced accelerations, the differential process indeed cancel the gravity-induced portions no matter what reading is. For example, equation (10) can be rewritten to

$$\begin{aligned} \dot{\omega}_x = & n((a_1 - a_{x,GC}) - (a_4 - a_{x,GC})) \\ & + n((a_2 - a_{y,GC}) - (a_5 - a_{y,GC})) \\ & + n((a_3 - a_{z,GC}) - (a_6 - a_{z,GC})) \end{aligned} \quad (11)$$

Therefore, the derivation of the angular acceleration in the proposed system is free of gravity effect. The system yields

correct angular acceleration even if the accelerometers don't go through gravity compensation process.

Though the measurements of angular acceleration and velocity are free of gravity effect, the linear acceleration is indeed affected by the gravity-induced acceleration. Thus, the pre-process of gravity compensation is required before the data can be imported into (9). A 2-axis inclinometer is utilized in the proposed system, which measures two tilting angles (θ_x , θ_y) between the principal axes of the body frame \mathcal{B} and the gravity vector in the representation of directional cosines. The third tilting angle θ_z can also be derived based on the property of direction cosines. Fig. 2 shows the angles defined by direction cosines, and θ_z can be obtained based on the property of, $\cos(\theta_x)^2 + \cos(\theta_y)^2 + \cos(\theta_z)^2 = 1$.

Thus, the gravity compensation terms a_{GC} is the projection of gravity on each axis of body frame \mathcal{B} , and can be derived by θ_x , θ_y , and θ_z :

$$\begin{aligned} a_{x,GC} &= g \cos(\theta_x) \\ a_{y,GC} &= g \cos(\theta_y), \\ a_{z,GC} &= g \cos(\theta_z) \end{aligned} \quad (12)$$

where g is the gravity constant.

The accurate accelerations a_j shown in (9) can be derived from the measurements of three 2-axis accelerometers a_{meas} minus the projected gravity vectors on the sensing directions a_{GC} at every instant.

$$a_j = a_{j,meas} - a_{j,GC}. \quad (13)$$

III. EXPERIMENTAL EVALUATION

A benchtop apparatus with one controllable rotational DOF shown in Fig. 1 was utilized for experimental evaluation of the proposed system. The required sensory measurements were obtained from three 3-axis accelerometers (ADXL330 [12], Analog Device, using 2-axis only), three 1-axis rate gyros (ADXRS610 [13], Analog Device), and one 2-axis inclinometer (SCA100T [14], VTI Technologies). In addition, a 3-axis accelerometer (ADXL330) was also mounted at COM for performance comparison (as the "traditional IMU"). The COM of the IMU system was positioned on the rotating apparatus with designated distance 30mm to the rotational axis along minus y-axis of the body frame \mathcal{B} , not at the rotation center of turntable as shown in Fig. 1. Thus, the simulated COM was subjected to tangential, normal, and angular accelerations while the turntable rotated. A realtime embedded control system (sBRIO-9632, National Instruments) running at 1kHz was in charge of sensor signal collection and sinusoidal position-controlled motion (amplitude 23.5° , frequency 1Hz). The rotating axis of the turntable was tilted 12° from the vertical axis, so the gravity-induced acceleration will affect all sensor readings in a time-variant manner, which provides a good scenario to evaluate the effectiveness of gravity compensation by the inclinometer.

Table 1 lists the root-mean-square (RMS) noises of the systems while the turntable is static. They are the means of

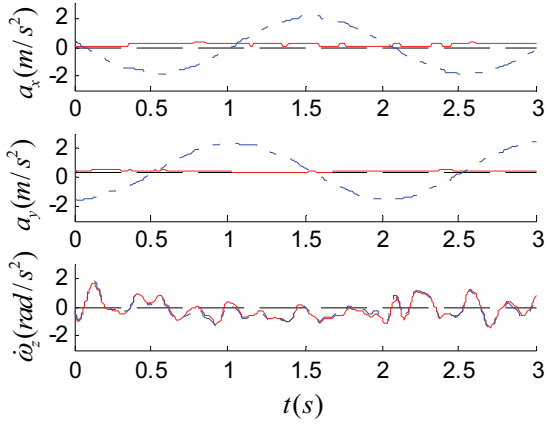


Figure 3. Comparison the states of 9-axis IMU system with and without gravity compensation (solid red vs. dashdot blue) while the apparatus rotated in constant velocity. The black dashed lines represent the theoretically estimated states. All of curves are filtered by hamming windows.

TABLE 1 RMS NOISE OF THE SYSTEMS WHILE STATIC

	linear acceleration (m/s^2)			Angular acceleration (rad/s^2)		
	a_x	a_y	a_z	$\dot{\omega}_x$	$\dot{\omega}_y$	$\dot{\omega}_z$
(a) Datasheet	0.0776	0.0776	0.0963			
(b) Traditional	0.0866	0.0808	0.1102	5.922	6.319	6.1928
(c) 9-axis	0.0749	0.0541	0.0752	0.6014	0.5815	0.5594

several experimental data sets. The left three columns list the COM linear acceleration: (a) is the nominal noise of the accelerometer itself [12]; (b) is the RMS error of the 3-axis accelerometers directly mounted at COM, which also presents the signal acquisition quality of the current mechatronic system; (c) is the RMS error derived from proposed 9-axis system, which clearly shows that redundancy of the sensors helps decreasing the noise. The right three columns show that the signal quality of angular acceleration derived from the 9-axis system is much better than that from traditional IMU which uses differentiation of gyro signals.

Fig. 3 shows the COM states of 9-axis IMU system with and without gravity compensation (solid red vs. dashdot blue) while the apparatus rotated in constant velocity and was tilted 12° . To make the plots presentable, data are filtered with hamming windows. The rotation speed is $180^\circ/s$. Due to 1 DOF rotation of the benchtop apparatus, the effective linear accelerations are two dimensional spanning in the plane perpendicular to rotational axis, the x-axis and y-axis of the body frame \mathcal{B} . The effective angular acceleration is along with the rotation axis, the z-axis of the body frame. The compensated linear accelerations (red solid) shown in the first and second subplots catch the trends of the ideal estimated states (black dash). While the uncompensated linear accelerations have sinusoidal states. The compensated and uncompensated angular accelerations in the third subplot are

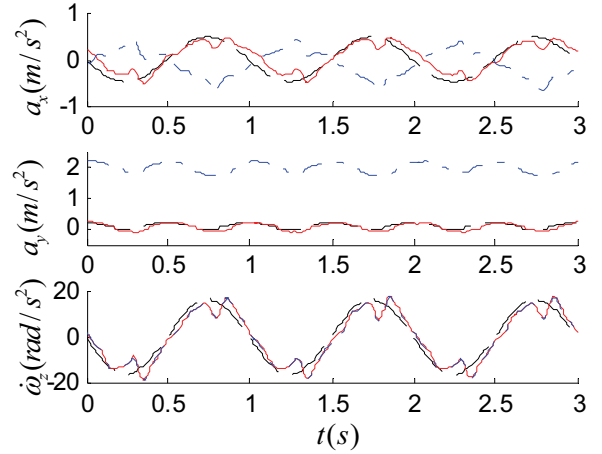


Figure 4. Comparison the states of 9-axis IMU system with and without gravity compensation (solid red vs. dashdot blue) while the apparatus rotated in sinusoidal motion. The black dashed lines represent the theoretically estimated states. All of curves are filtered by hamming windows.

identical since the angular acceleration is free of gravity effect in the 9-axis IMU system. Therefore it confirms that the gravity compensation of 9-axis IMU system is effective. The same phenomenal can be observed in Fig. 4 as well while the apparatus rotated in sinusoidal motion.

Fig. 5 compares the COM states of 9-axis IMU system (red solid) and the traditional IMU system (green dotted) while the apparatus rotated in sinusoidal motion. Both of the curves are filtered with hamming windows and are compensated with gravity. The linear accelerations along with x-axis and y-axis of body frame \mathcal{B} are plotted in the first and second subplots. The states of 9-axis IMU system catch the trends of traditional IMU systems. Thus, it confirms that the 9-axis IMU system can pride effective information as traditional IMU system. Comparing to the smooth ideal curves (black dashed), the experimental curves show vibrating behaviors because of position-based motion control and empirically unrigid apparatus structure, but in general the trends of the curves match each other. Since all systems use gyro to measure the angular velocity, in the 4th subplot only one experimental curve is plotted.

Fig. 6 shows the angular accelerations without filtering of 9-axis IMU system (solid red) and the traditional IMU system (dashed green) while the apparatus rotated in sinusoidal motion. Since the angular accelerations are derived by differential of angular velocity from gyro signals, noises are amplified via the process of differential. However, angular accelerations are derived by linear matrix computation. The qualities of obtained angular acceleration signals are much better than the traditional IMU system.

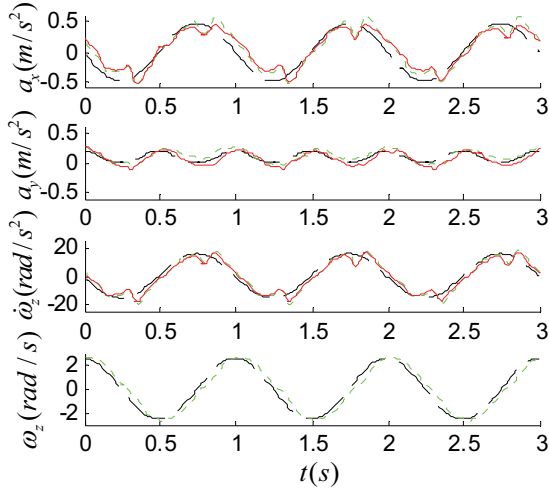


Figure 5. Comparison of state obtained from different methods: (a) black dashed line: ideal curve derived from desired position control trajectories; (b) green dashed line: derived from traditional IMU system with gravity compensation; (c) red solid line: derived from 9-axis system with gravity compensation; Figures from top to bottom are linear acceleration along x-axis of body frame B, linear acceleration along y-axis of body frame B, angular acceleration, and angular velocity, accordingly.

TABLE 2 RMS NOISE OF THE ANGULAR ACCELERATIONS WHILE SINUSOIDAL MOTION WITHOUT FILTERING.

	Angular acceleration (rad/s ²)		
	$\dot{\omega}_x$	$\dot{\omega}_y$	$\dot{\omega}_z$
(a) Traditional	6.3397	6.8002	10.3054
(b) 9-axis	1.5835	1.7003	6.5466

Table 2 shows the RMS noises of three angular accelerations. They are the means of several experimental data sets as well. The noise data of the 9-axis IMU system are derived with accelerometers and rate gyro measurements, and they show that redundancy of the sensors improves the signal qualities. It confirms the 9-axis IMU system can obtain more accurate angular acceleration signals than the traditional IMU system.

IV. CONCLUSION

We have investigated the performance of the 9-axis IMU with gravity compensation by utilizing an additional 2-axis inclinometer. The experimental results confirmed that the proposed system is capable of delivering desired linear acceleration, angular acceleration, and angular velocity states in normal gravitational environment.

The proposed 9-axis system with gravity compensation is also capable of deriving correct COM state of legged robots where the COM moves due to motions of the limbs. The procedure is listed below: (i) compute the desired states with respect to the nominal COM position defined as \mathbf{a}_c ; (ii) treat \mathbf{a}_{COM} as \mathbf{a}_p in (1), and obtain \mathbf{r}_{op} , $\dot{\mathbf{r}}_{op}$, and $\ddot{\mathbf{r}}_{op}$ related info by

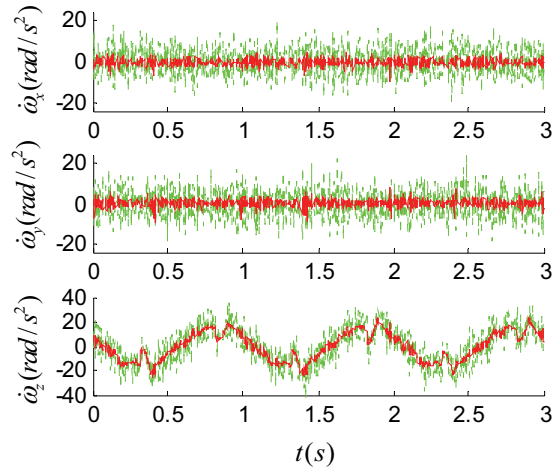


Figure 6. Comparison of angular acceleration without filtering obtained from different methods. The 9-axis IMU system (solid red) derived angular acceleration by linear matrix calculation, while the traditional IMU system (dashed green) derived it by differential of angular velocity.

robot joint sensors; (iii) compute \mathbf{a}_{COM} by (1). Because $\dot{\omega}$ of the proposed system is derived by (2), the numerical quality of computation of \mathbf{a}_{COM} by (1) in the step (iii) will not be deteriorated by differentiation as in the traditional IMU. We are currently implementing the algorithm on the robot to evaluate the performance.

ACKNOWLEDGMENT

The authors gratefully thank the National Instruments Taiwan Branch for their kindly support of equipments and technical consulting.

REFERENCES

- [1] N. Barbour and G. Schmidt, "Inertial sensor technology trends," *Sensors Journal*, vol. 1, pp. 332-339, 2001.
- [2] J. L. Weston and D. H. Titterton, "Modern inertial navigation technology and its application," *Electronics & Communication Engineering Journal*, vol. 12, pp. 49-64, 2000.
- [3] R. L. Greenspan, "Inertial navigation technology from 1970-1995," *Journal of the Institute of Navigation*, vol. 42, pp. 165-185, 1995.
- [4] B. Barshan and H. F. Durrantwhyte, "INERTIAL NAVIGATION SYSTEMS FOR MOBILE ROBOTS," *Ieee Transactions on Robotics and Automation*, vol. 11, pp. 328-342, 1995.
- [5] D. Giansanti, *et al.*, "Is it feasible to reconstruct body segment 3-D position and orientation using accelerometric data?," *Ieee Transactions on Biomedical Engineering*, vol. 50, pp. 476-483, Apr 2003.
- [6] W. T. Ang, *et al.*, "Nonlinear regression model of a low-g MEMS accelerometer," *Ieee Sensors Journal*, vol. 7, pp. 81-88, 2007.
- [7] P. Cappa, *et al.*, "Numerical validation of linear accelerometer systems for the measurement of head kinematics," *Journal of Biomechanical Engineering-Transactions of the Asme*, vol. 127, pp. 919-928, Nov 2005.
- [8] J. J. Crisco, *et al.*, "An algorithm for estimating acceleration magnitude and impact location using multiple nonorthogonal single-axis accelerometers," *Journal of Biomechanical Engineering-Transactions of the Asme*, vol. 126, pp. 849-854, Dec 2004.
- [9] P. C. Lin, *et al.*, "A leg configuration measurement system for full-body pose estimates in a hexapod robot (vol 21, pg 411, 2005)," *Ieee Transactions on Robotics*, vol. 21, pp. 778-778, Aug 2005.

- [10] P. C. Lin, *et al.*, "Sensor data fusion for body state estimation in a hexapod robot with dynamical gaits," *Ieee Transactions on Robotics*, vol. 22, pp. 932-943, Oct 2006.
- [11] P.-C. Lin and C.-W. Ho, "Design and Implementation of a 9-Axis Inertial Measurement Unit," in *IEEE International Conference on Robotics and Automation*, 2009, pp. 736-740.
- [12] (2010, *Analog Devices ADXL330 accelerometer datasheet*. Available: <http://www.analog.com/en/sensors/inertial-sensors/adxl330/products/product.html>
- [13] (2010, *Analog Devices ADXRS610 gyroscope datasheet*. Available: <http://www.analog.com/en/sensors/inertial-sensors/adxrs610/products/product.html>
- [14] (2010, *VTI Techmologies SCA100T inclinometer datasheet*. Available: <http://www.vti.fi/en/products/inclinometers/inclinometers/>